Tunable Size Dependence of Quantum Plasmon of Charged Gold Nanoparticles

Song Ma,[1,*] Da-Jie Yang,[2,3,*] Si-Jing Ding,[4,*] Jia Liu,[1] Wei Wang,[1] Zhi-Yong Wu,[1] Xiao-Dan Liu,[1] Li Zhou,[1,†] and Qu-Quan Wang[1,5,‡]

[1]*Key Laboratory of Artificial Micro-and Nano-structures of the Ministry of Education, School of Physics and Technology, Wuhan University, Wuhan 430072, China*

[2]*Department of Mathematics and Physics, North China Electric Power University, Beijing 102206, China*

[3]*Beijing Computational Science Research Center, Beijing 100193, China*

[4]*School of Mathematics and Physics, China University of Geosciences (Wuhan), Wuhan 430074, China*

[5]*The Institute for Advanced Studies, Wuhan University, Wuhan 430072, China*

(Received 11 November 2020; accepted 2 April 2021; published 30 April 2021)

The quantum behavior of surface plasmons has received extensive attention, benefiting from the development of exquisite nanotechnology and the diverse applications. Blueshift, redshift, and nonshift of localized surface plasmon resonances (LSPRs) have all been reported as the particle size decreases and enters the quantum size regime, but the underlying physical mechanism to induce these controversial size dependences is not clear. Herein, we propose an improved semiclassical model for modifying the dielectric function of metal nanospheres by combining the intrinsic quantized electron transitions and surface electron injection or extraction to investigate the plasmon shift and LSPR size dependence of the charged Au nanoparticles. We experimentally observe that the nonmonotonic blueshift of LSPRs with size for Au nanoparticles is turned into an approximately monotonic blueshift by increasing the electron donor concentration in the reduction solution, and it can also be transformed to an approximately monotonic redshift after surface passivation by ligand molecules. Moreover, we demonstrate controlled blueshift and redshift for the electron and hole plasmons in $Cu_{2-x}S$@Au core-shell nanoparticles by injecting electrons. The experimental observations and the theoretical calculations clarify the controversial size dependences of LSPR reported in the literature, reveal the critical role of surface electron injection or extraction in the transformation between the different size dependences of LSPRs, and are helpful for understanding the nature of surface plasmons in the quantum size regime.

DOI: 10.1103/PhysRevLett.126.173902

Intense effort has been devoted to tuning the collective electron excitation, named plasmon resonance, of metal nanostructures with precisely controlled sizes and shapes in various environments [1], which has immediate significance for diverse applications ranging from quantum information to photocatalysis and biospectroscopy [2]. Benefiting from the development of exquisite nanotechnology, especially the excitation of plasmons by an electron beam with high spatial resolution [3], the quantum behavior of both propagating [4] and localized plasmons [5] has attracted great interest recently. In particular, plasmon resonance shifting, broadening, and splitting for metal nanostructures in the quantum size regime have been extensively studied [6–12].

The size-dependent localized surface plasmon resonances (LSPRs) of spherical metal nanoparticles with the simplest geometry are fundamental for understanding the plasmonic nature and have been investigated for several decades [13–17]. However, the size dependences of LSPRs reported in the existing literature are highly controversial, and the underlying dominant physical mechanism is under serious debate [18–22]. For instance, both redshifting and blueshifting of LSPRs were observed when the particle size decreases and enters the quantum size regime [23–26]. When decreasing the size of silver nanoparticles (AgNPs), size-independent LSPRs with photon excitation and a blueshifting size dependence with electron beam excitation were reported very recently [27].

As a pathway leading to LSPR shift, electron injection or extraction is a universal phenomenon that exists in the wet-chemical synthesis (e.g., gain of electrons under atom reduction in growth and loss of electrons under atom oxidation in etching), as well as in the annealing processes of a solid matrix or in the LSPR measurement by electron beam excitation; however, a comprehensive understanding of the regulation of the LSPR size dependence by electron injection or extraction is absent. A theoretical model and analysis for the plasmon shift of the charged metal nanoparticles and experimental demonstration of the transformation of LSPR size dependence are highly desirable.

In this Letter, we propose an improved semiclassical model for modifying the dielectric function of metal nanospheres by combining the intrinsic quantized electron transitions and surface charge transfer to investigate

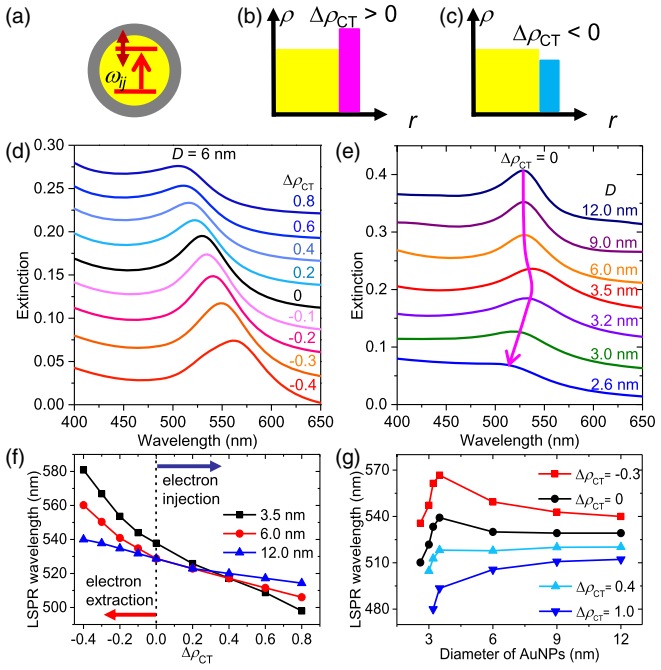

FIG. 1. Hard boundary box model of charged AuNPs and calculated extinction spectra. (a) Core-shell model of AuNP. (b) Electron is injected into the surface layer of Au ($\Delta\rho_{CT} > 0$). (c) Electron is extracted from the surface layer of Au ($\Delta\rho_{CT} < 0$). (d) Calculated LSPRs of AuNPs ($D = 6$ nm) with different $\Delta\rho_{CT}$. (e) Calculated LSPRs of AuNPs with different diameters ($\Delta\rho_{CT} = 0$). (f) LSPR wavelength of AuNPs ($D = 3.5$, 6.0, and 12.0 nm) with varied $\Delta\rho_{CT}$. (g) LSPR size dependences of AuNPs with $\Delta\rho_{CT} = -0.3$, 0, 0.4, and 1.0.

plasmon shift and LSPR size dependence of the charged AuNPs. Experimentally, we observe that the size-dependent LSPR for AuNPs is gradually transformed from a nonmonotonic blueshift to an approximately monotonic blueshift by increasing the electron donor concentration during reduction growth of AuNPs, and to an approximately monotonic redshift after surface passivation by ligand molecules. Moreover, the charge transfer effect is well demonstrated by injecting electrons into $Cu_{2-x}S$@Au core-shell nanoparticles, in which the electron and hole plasmons are controlled to blueshift and redshift. The observed transformation of the size-dependent LSPRs is well explained by the modified theoretical model.

We at first theoretically investigate the plasmon shifts of AuNPs induced by surface charge transfer. The electron injection or extraction associated with the AuNPs, as well as the electron density distributions of the charged AuNPs, are described by a modified hard boundary box model. As shown in Figs. 1(a)–1(c), the fluctuation in the electron density within the AuNPs is assumed to be located at the outermost layer of atoms, which is described by a shell with a thickness (d_s) of 0.5 nm in the calculations [6]. The normalized density of injected electrons within the shell is described by $\Delta\rho_{CT} = (\rho_s - \rho_c)/\rho_c$, where ρ_s and ρ_c are the electron densities of the core and shell, respectively. For simplification and clarity, the perturbation of the refractive index change of the surrounding environment is not taken into account in the calculations.

The dielectric function of AuNP is modeled by the sum of ϵ_{intra} and ϵ_{inter}. The interband part ϵ_{inter} is modeled using random phase approximation [28]. The intraband part ϵ_{intra} is described by the Drude model incorporating quantum transitions $S_{if} = 2M\omega_{if}\langle f|z|i\rangle^2/\hbar N$ [13,26] (see Sec. 1.1 in the Supplemental Material [29]), where ω_{if} is the frequency of the transition from initial state i to final state f of the conduction electrons. M is the electron mass and N is the electron number. The change of surface electron density (injection with $\Delta\rho_{CT} > 0$ or extrication with $\Delta\rho_{CT} < 0$) will significantly influence the bulk plasma frequency ω_p and the LSPR frequency as well as the Fermi level, see Fig. S1 in the Supplemental Material [29]. With the dielectric functions of core and shell materials calculated separately (see Sec. 1.2 in Supplemental Material [29]), the optical spectra are then calculated using Mie scattering theory. Both ω_{if} and S_{if} are strongly dependent on the size, which leads to oscillations of LSPR wavelength with the size [13]. Figure 1(d) shows the dependence of extinction spectra as a function of $\Delta\rho_{CT}$ for an AuNP with the diameter $D = 6.0$ nm. The extinction spectra exhibit an obvious blueshift with $\Delta\rho_{CT}$ varying from -0.4 to 0.8. A smaller AuNP has a larger surface area to volume ratio and is more sensitive to electron injection or extraction. As shown in Fig. 1(f), when $\Delta\rho_{CT}$ increases from -0.4 to 0.8, the calculated λ_{LSPR} of the smaller AuNPs with $D = 3.5$ nm decreases by 82.9 nm, whereas that of the larger AuNPs with $D = 12.0$ nm only decreases by 25.7 nm.

The size-dependent quantum plasmon behavior in Figs. 1(e) and S2 of Ref. [29] with no charge transfer ($\Delta\rho_{CT} = 0$) shows a nonmonotonic shift as the previous report [13]. Interestingly, the LSPR size dependence is transformed from a nonmonotonic shift to an approximately monotonic blueshift when $\Delta\rho_{CT}$ is increased to 1.0 [Figs. 1(g) and S3 [29]]. It indicates that the electron injection makes the LSPR shift in the high-energy direction. As a result, LSPR size dependence is tuned by the electron injection or extraction.

Then, we experimentally explore the plasmon shifts of the AuNPs by introducing electron donors or acceptors. Uniform colloidal AuNPs were prepared in an aqueous solution by using a reduction reaction of $HAuCl_4$ with ascorbic acid (AA) in the presence of Au seeds and hexadecyl-trimethyl-ammonium bromide (CTAB) [30]. The AuNPs stabilized by CTAB molecules are individually suspended in the solutions [31–34]. The diameter of AuNPs synthesized by overgrowth of Au on the seeds can be estimated from the volume V_{Au+} of $HAuCl_4$ added in the reduction reaction [Figs. S4(a)–4(f) Supplemental Material [29]], and the diameter of Au in this following study refers to nominal diameter (D_{Nom}) with the

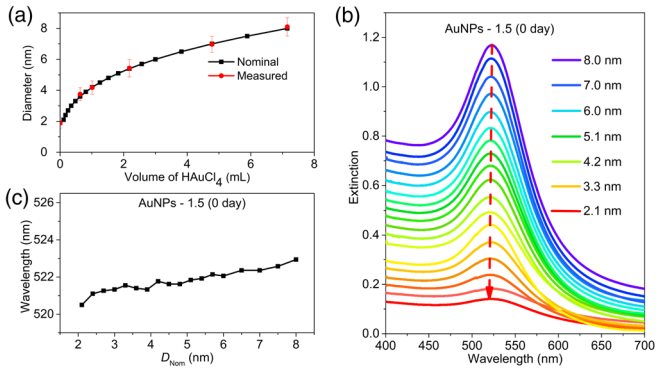

FIG. 2. Nonmonotonic-shifting LSPR size dependence of AuNPs synthesized by a reduction reaction. (a) Measured and nominal sizes (D and D_{Nom}) of AuNPs prepared with various volumes of $HAuCl_4$ ($V_{\mathrm{Au+}}$). (b) Size-dependent extinction spectra of AuNPs with $m_{\mathrm{AA}}/m_{\mathrm{Au+}} = 1.5$ ($D_{\mathrm{Nom}} = 2.1$–8.0 nm). The spectra are vertically shifted for clarity. (c) Size dependence of the plasmon resonance wavelength of the AuNPs synthesized with $m_{\mathrm{AA}}/m_{\mathrm{Au+}} = 1.5$.

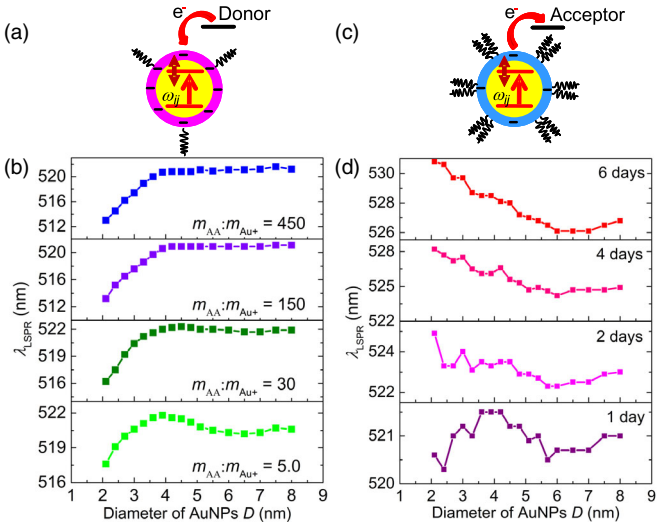

FIG. 3. LSPR size dependences of AuNPs with electron injection and electron extraction. (a) Schematic illustration of electron injection from electron donors (AA) to AuNPs. (b) Schematic illustration of electron extraction from AuNPs to ligand molecules. (c) The LSPR size dependence is gradually transformed from the nonmonotonic shift to an approximately monotonic blueshift when the value of $m_{\mathrm{AA}}/m_{\mathrm{Au+}}$ increases from 5.0 to 450 (0 day). (d) The LSPR size dependence is gradually transformed from the nonmonotonic shift to an approximately monotonic redshift when the passivation time increases from 1 to 6 days ($m_{\mathrm{AA}}/m_{\mathrm{Au+}} = 5.0$).

relationship $D_{\mathrm{Nom}} = [(D_0)^3 + bV_{\mathrm{Au+}}]^{1/3}$, where D_0 is the diameter, measured as 1.9 ± 0.3 nm, of the Au seeds, and b is calculated to be 0.071 $\mathrm{nm}^3/\mu\mathrm{L}$ [Fig. 2(a)]. The recorded extinction spectra of the AuNPs with $D_{\mathrm{Nom}} = 2.1$–8.0 nm demonstrate a slight blueshift of LSPR with size under a low electron donor molar ratio ($m_{\mathrm{AA}}/m_{\mathrm{Au+}} = 1.5$), see Figs. 2(b) and 2(c).

An excess reductant of AA molecules was added as electron donors to inject electrons into the AuNPs, and $m_{\mathrm{AA}}/m_{\mathrm{Au+}}$ was used to evaluate the effect of electron injection. The measured zeta-potential decreases as $m_{\mathrm{AA}}/m_{\mathrm{Au+}}$ increases (Fig. S5 of the Supplemental Material [29]), which indicates that the electrons are transferred from the AA molecules to the AuNPs [Fig. 3(a)] and lead to a blueshift of the LSPR. Figure 3(b) comparatively presents the size-dependent LSPRs of the AuNPs synthesized with $m_{\mathrm{AA}}/m_{\mathrm{Au+}} = 5.0$, 30, 150, and 450. As $m_{\mathrm{AA}}/m_{\mathrm{Au+}}$ increases from 1.5 to 450, the λ_{LSPR} of the smaller AuNPs with $D_{\mathrm{Nom}} = 2.1$ nm decreases by 7.5 nm, whereas that of the larger AuNPs with $D_{\mathrm{Nom}} = 6.0$ nm slightly decreases by 1.0 nm [Fig. S4(g) [29]]. This indicates that the LSPR wavelength of the smaller AuNPs is more sensitive to electron injection. The electron injection effect is further demonstrated on a kind of etched AuNPs, which show a more prominent blueshift using a postaddition method of electron donors [Fig. S7 [29]].

A nonmonotonically shifting LSPR size dependence is observed when $m_{\mathrm{AA}}/m_{\mathrm{Au+}}$ is 5.0 [bright green curve in Fig. 3(b)], which is attributed to the collaboration of size-dependent quantum transitions in the conduction band and damping of free electrons [26]. The maximum λ_{LSPR} is around $D_{\mathrm{Nom}} = 3.9$ nm. This oscillation of the plasmon resonance wavelength is similar to that reported for individual AgNPs [13]. However, the oscillation of the LSPR wavelength with the AuNP size becomes weak when $m_{\mathrm{AA}}/m_{\mathrm{Au+}}$ increases, and it is hard to observe when $m_{\mathrm{AA}}/m_{\mathrm{Au+}}$ increases to 450. With higher $m_{\mathrm{AA}}/m_{\mathrm{Au+}}$, the LSPR shift is dominated by electron injection, and the LSPR oscillation is suppressed. Consequently, the LSPR size dependence is transformed from the nonmonotonic shift to a monotonic blueshift. This indicates that the electron injection from the donor to the AuNPs significantly modulates LSPR size dependence.

In contrast, a redshift of LSPR is observed for the AuNPs after surface passivation in the original synthesis solution owing to electron extraction from the surface of the AuNPs to the capping ligand molecules [Fig. 3(c)] [6]. This natural passivation process lasts for several days and commonly exists in wet-chemical synthesis [31,32,35], and the adsorbed ligands during the passivation process are directly observed in the transmission electron microscope (TEM) images (Fig. S6 [29]). After 6 days of passivation, the λ_{LSPR} of smaller AuNPs with $D_{\mathrm{Nom}} = 2.1$ nm significantly increases by 13.2 nm, whereas that of the larger AuNPs with $D_{\mathrm{Nom}} = 6.0$ nm increases by 5.8 nm (Fig. S4(h) [29]). The LSPR size dependence is transformed from the nonmonotonic shift to an approximately monotonic redshift for the samples with more than two days of passivation [Fig. 3(d)].

The redshifting LSPR size dependence of AuNPs is similar to that of AgNPs interpreted by a multilayer Mie

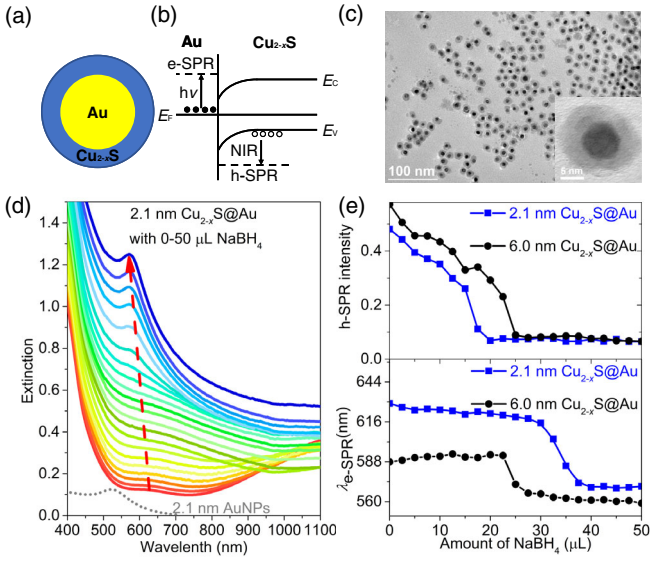

FIG. 4. LSPR blueshift of $Cu_{2-x}S$@Au heteronanostructures with electron injection. (a),(b) Schematic illustration of the $Cu_{2-x}S$@Au core-shell heteronanostructure and band alignment. (c) TEM images of $Cu_{2-x}S$@Au with $D_{Au} = 7.5 \pm 0.4$ nm and average $Cu_{2-x}S$ shell thickness of 5 nm. (d) Extinction spectra of $Cu_{2-x}S$@Au ($D_{Au} = 2.1$ nm) prepared with various volumes of $NaBH_4$ as the electron donor. The volume of 1 M $NaBH_4$ is gradually increased from 2.5 μL to 50 μL. The gray dotted line refers to the original extinction spectrum of AuNPs with diameter of 2.1 nm. The spectra are vertically shifted for clarity. (e) The h-SPR intensity at 1100 nm and e-SPR wavelength as a function of the $NaBH_4$ volume of $Cu_{2-x}S$@Au with $D_{Au} = 2.1$ nm and $D_{Au} = 6.0$ nm.

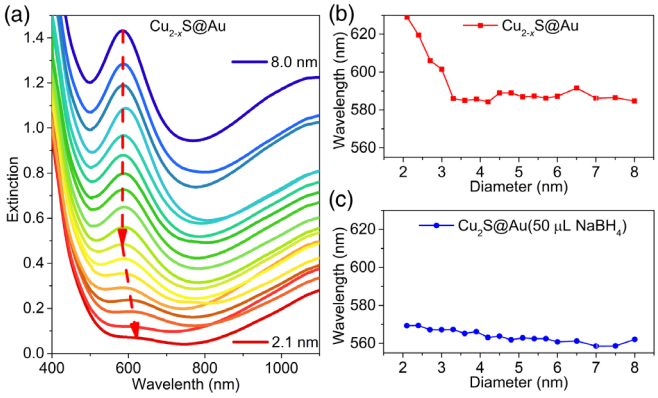

FIG. 5. LSPR size dependences of $Cu_{2-x}S$@Au and Cu_2S@Au. (a) Size-dependent extinction spectra of $Cu_{2-x}S$@Au with D_{Au} varying from 8.0 to 2.1 nm (without adding $NaBH_4$). The spectra are vertical shifted for clarity. (b),(c) LSPR size dependences of $Cu_{2-x}S$@Au and Cu_2S@Au (reduced by 50 μL $NaBH_4$).

theory model considering the influence of an outermost atomic layer with lowered electron conductivity [6]. The redshift of the plasmon resonance can be explained by the gradual adsorption of the ligand molecules onto the surface of colloidal AuNPs in the surface passivation process. The increased ligand molecules and the electron extraction from the surface of AuNPs to the adsorbed ligand molecules lead to a decrease in the electron density and then a redshift of LSPR. Additionally, the adsorbed ligand molecules increase the refractive index of the local environment around the AuNPs, which also leads to a redshift of the LSPR.

To further explore the influence of charge transfer on the LSPR of AuNPs, $Cu_{2-x}S$ was overgrown on different size AuNPs [Figs. 4(a)–4(c)] [36,37]. $Cu_{2-x}S$ with Cu deficiencies is a self-doped p-type semiconductor that has sufficient carrier density to support LSPR with the collective oscillation of holes in the near infrared (NIR) region [38,39]. After overgrowing $Cu_{2-x}S$ semiconductor shells on the AuNPs, free electrons on the surface of the AuNPs diffuse to $Cu_{2-x}S$ [40–42]. As a result, the density of free electrons on the surface of the AuNPs is prominently decreased.

Typical TEM images of $Cu_{2-x}S$@Au in Figs. 4(c) and S8 of the Ref. [29] show that the average thickness of the $Cu_{2-x}S$ shell is 5.0 nm. The extinction spectra of $Cu_{2-x}S$@Au with Au core diameters of $D_{Au} = 2.1$ and 6.0 nm under the gradual addition of $NaBH_4$ (1 M, as the electron donor) are shown in Figs. 4(d) and S9(a), respectively. With the increase of reductant $NaBH_4$, the self-doped semiconductor $Cu_{2-x}S$ shell was gradually transformed to Cu_2S, and the NIR LSPR of $Cu_{2-x}S$ gradually vanished and slightly redshifted [Fig. S9(b) [29]], because of the decrease in free holes. The measured intensity of the hole-induced SPR (h-SPR) in $Cu_{2-x}S$ and the wavelength of the electron-induced SPR (e-SPR) in gold are presented in Fig. 4(e) to exhibit the spectral evolution induced by electron injection. In the range of 0 to 25 μL $NaBH_4$, the h-SPR intensity gradually decreased while the e-SPR wavelength was little altered. Only the peripheral $Cu_{2-x}S$ is speculated to be reduced in this range. With further increase in $NaBH_4$, electrons start to be injected into gold across the interface of $Cu_{2-x}S$@Au. In the range of 25 to 50 μL $NaBH_4$, the h-SPR intensity of $Cu_{2-x}S$ remains zero because all the $Cu_{2-x}S$ has been reduced to Cu_2S, while the e-SPR wavelength of gold gradually blueshifts and the e-SPR intensity gradually increases due to the rise of the electron concentration at the surface of the AuNPs. The initial $Cu_{2-x}S$@Au with $D_{Au} = 2.1$ nm has a very weak e-SPR, and the e-SPR is significantly enhanced and blueshifted by 59 nm after 50 μL of $NaBH_4$ is added. For the larger $Cu_{2-x}S$@Au with $D_{Au} = 6.0$ nm, the e-SPR wavelength blueshifts by 29 nm. Similarly, $Cu_{2-x}S$@Au with a smaller Au core is more sensitive to the electron injection effect as well as the local environment.

Figure 5(a) displays the LSPR size dependence of $Cu_{2-x}S$@Au. As D_{Au} decreases from 8.0 to 2.1 nm, the e-SPR wavelength of gold first fluctuates around approximately 585.0 nm and then greatly redshifts to 629.0 nm.

This result implies that under the same conditions of growing a 5.0 nm $Cu_{2-x}S$ shell, the smaller AuNPs lose relatively more electrons due to the hole diffusion originating from $Cu_{2-x}S$, resulting in great redshifting and damping of the e-SPR. Figures 5(b) and S10 [29] also show the LSPR size dependence of Cu_2S@Au (reduced from $Cu_{2-x}S$@Au by $NaBH_4$). The e-SPR wavelength of gold only slightly redshifts from 569.3 to 562.1 nm. This slight redshift originates from the increased effective refractive index of the Cu_2S dielectric shell.

Finally, we mentioned that the observed plasmon shifts, such as the plasmon blueshifting caused by introducing an electron donor of AA and the plasmon redshifting caused by electron extraction to CTAB ligand molecules or *p*-type $Cu_{2-x}S$, as well as the LSPR size dependences, can be well explained by the calculation from the modified model. Furthermore, for the electron-beam-excited LSPR of ligand-free metal nanoparticles on a substrate or embedded in a matrix, electron injection or extraction between the nanoparticles and the ligand molecules is avoided, but an appropriate dose of electrons will increase the surface electron density of the metal nanoparticles. Therefore, the electron injection or extraction model can also well explain the prominent plasmon blueshift and the quantum oscillations with the size of the metal nanoparticles excited by electrons. It also straightforwardly explains the large discrepancy in the size-dependent LSPR excited by photons and electrons, and can be further extended to address plasmonic nanoparticles involving redox processes. Note that our simplified model can be extended to calculate the plasmon shifts caused by carrier diffusion, such as interfacial charge transfer of metal-semiconductor heteronanostructures, and roughly discuss the influence of the spill-out effect (Fig. S11 of Ref. [29]) [27]. Many interfacial interactions, such as work function and chemical bond, are not involved in our simplified model. Electron transfer dynamics of small-sized metal nanoparticles can be revealed by using time-dependent density functional theory (TDDFT) [43–45], and the improvement on the theoretical model remains to be further studied.

In conclusion, we propose a modified hard boundary box model to study the quantum plasmon mechanism of charged AuNPs. The electron injection or extraction process is described by controlling the charge transfer between the Au core and ligand shell, which change the concentration of conducting electrons and influence the intrinsic quantized electron transitions. After introducing this effect into the semiclassical model, the nonmonotonic shift of the LSPR with the size of the AuNPs at a low electron donor concentration and the monotonic blueshift at a high electron donor concentration, as well as the monotonic redshift after passivation, are well explained by the calculated extinction spectra from the theoretical model. Furthermore, by injecting electrons into $Cu_{2-x}S$@Au, the electron and hole plasmons are controlled to blueshift and redshift, which reveals that the surface electron injection or extraction process significantly influences the size dependence of LSPRs. This study offers a strategy to manipulate LSPR size dependence of the quantum-sized metal nanoparticles via surface charge transfer and can be applied to investigating plasmon resonances under electron beam excitation or optical excitation while contributing to the research on quantum plasmons.

We thank Dr. Yun-Hang Qiu and Dr. Kai Chen for the help of sample characterization and data analysis. This work was supported by the National Key R&D Program of China (Grants No. 2017YFA0303402 and No. 2020YFA0211300), and the National Natural Science Foundation of China (Grants No. 11874293, No. 12074296, and No. 11904332).

*These authors have contributed equally to this work.
†zhouli@whu.edu.cn
‡qqwang@whu.edu.cn

[1] L. Scarabelli, M. Coronado-Puchau, J. J. Giner-Casares, J. Langer, and L. M. Liz-Marzán, ACS Nano **8**, 5833 (2014); N. R. Jana, L. Gearheart, and C. J. Murphy, J. Phys. Chem. B **105**, 4065 (2001); R. Jiang, F. Qin, Y. Liu, X. Y. Lin, J. Guo, M. Tang, S. Cheng, and J. Wang, Adv. Mater. **28**, 6322 (2016); Y. H. Qiu, S. J. Ding, Y. J. Lin, K. Chen, D. J. Yang, S. Ma, X. L, H. Q. Lin, J. Wang, and Q. Q. Wang, ACS Nano **14**, 736 (2020); Q. Ding, Y. Shi, M. Chen, H. Li, X. Yang, Y. Qu, W. Liang, and M. Sun, Sci. Rep. **6**, 32724 (2016); M. Z. Ge, C. Y. Cao, S. H. Li, Y. X. Tang, L. N. Wang, N. Qi, J. Y. Huang, K. Q. Zhang, S. S. Al-Deyab, and Y. K. Lai, Nanoscale **8**, 5226 (2016); I. Pastoriza-Santos, A. Sánchez-Iglesias, B. Rodríguez-González, and L. M. Liz-Marzán, Small **5**, 440 (2009).

[2] J. Zhang, Y. Tang, K. Lee, and M. Ouyang, Nature (London) **466**, 91 (2010); C. Clavero, Nat. Photonics **8**, 95 (2014); S. Aksu, A. E. Cetin, R. Adato, and H. Altug, Adv. Opt. Mater. **1**, 798 (2013).

[3] M. Kociak and O. Stéphana, Chem. Soc. Rev. **43**, 3865 (2014); C. Colliex, M. Kociak, and O. Stéphana, Ultramicroscopy **162**, A1 (2016); Y. Wu, G. Li, and J. P. Camden, Chem. Rev. **118**, 2994 (2018); E. Pomarico, Y. J. Kim, F. J. G. de Abajo, O. H. Kwon, F. Carbone, and R. M. van der Veen, MRS Bull. **43**, 497 (2018).

[4] E. Altewischer, M. P. van Exter, and J. P. Woerdman, Nature (London) **418**, 304 (2002); E. Moreno, F. J. García-Vidal, D. Erni, J. Ignacio-Cirac, and L. Martín-Moreno, Phys. Rev. Lett. **92**, 236801 (2004); S. Fasel, F. Robin, E. Moreno, D. Erni, N. Gisin, and H. Zbinden, Phys. Rev. Lett. **94**, 110501 (2005); F. Ren, G. P. Guo, Y. F. Huang, C. F. Li, and G. C. Guo, Europhys. Lett. **76**, 753 (2006); e) Guo, X. F. Ren, Y. F. Huang, C. F. Li, Z. Y. Ou, and G. C. Guo, Phys. Lett. A **361**, 218 (2007); A. Huck, S. Smolka, P. Lodahl, A. S. Sørensen, A. Boltasseva, J. Janousek, and U. L. Andersen, Phys. Rev. Lett. **102**, 246802 (2009); Z. Yuan and S. Gao, Phys. Rev. B **73**, 155411 (2006); S. Thongrattanasiri, A. Manjavacas, and F. J. G. de Abajo, ACS Nano **6**, 1766 (2012).

[5] F. Ouyang, P. E. Batson, and M. Isaacson, Phys. Rev. B **46**, 15421 (1992); N. J. Halas, S. Lal, W. S. Chang, S. Link, and

P. Nordlander, Chem. Rev. **111**, 3913 (2011); W. P. Halperin, Rev. Mod. Phys. **58**, 533 (1986); L. Genzel, T. P. Martin, and U. Kreibig, Z. Phys. B **21**, 339 (1975); R. Liu, Z. K. Zhou, Y. C. Yu, T. Zhang, H. Wang, G. Liu, Y. Wei, H. Chen, and X. H. Wang, Phys. Rev. Lett. **118**, 237401 (2017); Z. C. Dong, X. L. Zhang, H. Y. Gao, Y. Luo, C. Zhang, L. G. Chen, R. Zhang, X. Tao, Y. Zhang, J. L. Yang, and J. G. Hou, Nat. Photonics **4**, 50 (2010).

[6] S. Peng, J. M. McMahon, G. C. Schatz, S. K. Gray, and Y. Sun, Proc. Natl. Acad. Sci. U.S.A. **107**, 14530 (2010).

[7] H. J. Qin, Y. Gao, J. Teng, H. X. Xu, K. H. Wu, and S. W. Gao, Nano Lett. **10**, 2961 (2010).

[8] M. J. Rice, W. R. Schneider, and S. Strässler, Phys. Rev. B **8**, 474 (1973).

[9] P. Apell and Å. Ljungbert, Phys. Scr. **26**, 113 (1982).

[10] J. Zuloaga, E. Prodan, and P. Nordlander, ACS Nano **4**, 5269 (2010).

[11] M. Zapata-Herrera, J. Flórez, A. S. Camacho, and H. Y. Ramírez, Plasmonics **13**, 1 (2018).

[12] C. F. A. Negre, E. M. Perassi, E. A. Coronado, and C. G. Sánchez, J. Phys. Condens. Matter **25**, 125304 (2013).

[13] J. A. Scholl, A. L. Koh, and J. A. Dionne, Nature (London) **483**, 421 (2012).

[14] S. Razaa, N. Stengera, S. Kadkhodazadeh, S. V. Fischer, N. Kostesha, A. P. Jauho, A. Burrows, M. Wubs, and N. A. Mortensen, Nanophotonics **2**, 131 (2013).

[15] A. Hilger, N. Cüppers, M. Tenfelde, and U. Kreibig, Eur. Phys. J. D **10**, 115 (2000).

[16] T. Christensen, W. Yan, S. Raza, A. P. Jauho, N. A. Mortensen, and M. Wubs, ACS Nano **8**, 1745 (2014).

[17] S. Raza, S. Kadkhodazadeh, T. Christensen, M. D. Vece, M. Wubs, N. A. Mortensen, and N. Stenger, Nat. Commun. **6**, 8788 (2015).

[18] H. Haberland, Nature (London) **494**, E1 (2013).

[19] A. Liebsch, Phys. Rev. B **48**, 11317 (1993).

[20] C. Bréchignac, P. Cahuzac, J. Leygnier, and A. Sarfati, Phys. Rev. Lett. **70**, 2036 (1993).

[21] M. Hillenkamp, G. D. Domenicantonio, O. Eugster, and C. Félix, Nanotechnology **18**, 015702 (2007).

[22] N. A. Mortensen, S. Raza, M. Wubs, T. Sndergaard, and S. I. Bozhevolnyi, Nat. Commun. **5**, 3809 (2014).

[23] R. C. Monreal, T. J. Antosiewicz, and S. P. Apell, New J. Phys. **15**, 083044 (2013).

[24] S. Raza, W. Yan, N. Stenger, M. Wubs, and N. A. Mortensen, Opt. Express **21**, 27344 (2013).

[25] A. L. Koh, K. Bao, I. Khan, W. E. Smith, G. Kothleitner, P. Nordlander, S. A. Maier, and D. W. McComb, ACS Nano **3**, 3015 (2009).

[26] S. J. Ding, D. J. Yang, J. L. Li, G. M. Pan, L. Ma, Y. J. Lin, J. H. Wang, L. Zhou, M. Feng, H. Xu, S. Gao, and Q. Q. Wang, Nanoscale **9**, 3188 (2017).

[27] A. Campos, N.Troc, E. Cottancin, M. Pellarin, H. C. Weissker, J. Lermé, M. Kociak, and M. Hillenkamp, Nat. Phys. **15**, 275 (2019).

[28] G. P. Wiederrecht, G. A. Wurtz, and J. Hranisavljevic, Nano Lett. **4**, 2121 (2004).

[29] See Supplemental Material at http://link.aps.org/supplemental/10.1103/PhysRevLett.126.173902 for details of theoretical model, data, discussions, and figures.

[30] Y. Zheng, X. Zhong, Z. Li, and Y. Xia, Part. Part. Syst. Charact. **31**, 266 (2014).

[31] H. Chen, L. Shao, Q. Li, and J. Wang, Chem. Soc. Rev. **42**, 2679 (2013).

[32] P. Pramod and K. G. Thomas, Adv. Mater. **20**, 4300 (2008).

[33] Y. J. Yang and W. Li, Biosens. Bioelectron. **56**, 300 (2014).

[34] R. Hosseinzadeha, R. E. Sabzi, and K. Ghasemlub, Colloids Surf. B **68**, 213 (2009).

[35] N. D. Burrows, W. Lin, J. G. Hinman, J. M. Dennison, A. M. Vartanian, N. S. Abadeer, E. M. Grzincic, L. M. Jacob, J. Li, and C. J. Murphy, Langmuir **32**, 9905 (2016).

[36] Y. Yang, S. Han, G. Zhou, L. Zhang, X. Li, C. Zou, and S. Huang, Nanoscale **5**, 11808 (2013).

[37] L. Ma, S. Liang, X. L. Liu, D. J. Yang, L. Zhou, and Q. Q. Wang, Adv. Funct. Mater. **25**, 898 (2015).

[38] P. H. Liua, M. Wenb, C. S. Tana, M. Navlani-Garcíab, Y. Kuwaharab, K. Morib, H. Yamashitab, and L. J. Chen, Nano Energy **31**, 57 (2017).

[39] Y. Xie, A. Riedinger, M. Prato, A. Casu, A. Genovese, P. Guardia, S. Sottini, C. Sangregorio, K. Miszta, S. Ghosh, T. Pellegrino, and L. Manna, J. Am. Chem. Soc. **135**, 17630 (2013).

[40] T. A. Patel and E. Panda, Appl. Surf. Sci. **488**, 477 (2019).

[41] J. O. McCaldin, T. C. McGill, and C. A. Mead, Phys. Rev. Lett. **36**, 56 (1976).

[42] D. Ding, K. Liu, S. He, C. Gao, and Y. Yin, Nano Lett. **14**, 6731 (2014).

[43] C. Lian, S. Q. Hu, J. Zhang, C. Cheng, Z. Yuan, S. Gao, and S. Meng, Phys. Rev. Lett. **125**, 116802 (2020).

[44] J. Yan, Z. Yuan, and S. Gao, Phys. Rev. Lett. **98**, 216602 (2007).

[45] M. Ludwig, G. Aguirregabiria, F. Ritzkowsky, T. Rybka, D. C. Marinica, J. Aizpurua, A. G. Borisov, A. Leitenstorfer, and D. Brida, Nat. Phys. **16**, 341 (2020).